

Article

Al₂O₃ nanorod with rich pentacoordinate Al³⁺ sites stabilizing Co²⁺ for propane dehydrogenation

Zhiping Zhao ¹, Yanbing Tong ², Jinru Sun ³, Ming Ke ^{4,*} and Weiyu Song ^{5,*}

¹ State Key Laboratory of Heavy Oil Processing, China University of Petroleum, Beijing 102249, China.; zhao920604@163.com

² State Key Laboratory of Heavy Oil Processing, China University of Petroleum, Beijing 102249, China.; 15010095354@163.com

³ State Key Laboratory of Heavy Oil Processing, China University of Petroleum, Beijing 102249, China.; sunjinru32@163.com

⁴ State Key Laboratory of Heavy Oil Processing, China University of Petroleum, Beijing 102249, China.; kemeng_0824@163.com

⁵ State Key Laboratory of Heavy Oil Processing, China University of Petroleum, Beijing 102249, China.; songwy@cup.edu.cn

Abstract: Co-based catalysts have gained significant attention in recent years due to their excellent ability to activate C-H bonds and high selectivity towards olefins, despite being a non-noble and environmentally unfriendly metal. However, further improvements are necessary for practical utilization, particularly in terms of activity and anti-carbon deposition capacity. In this study, we synthesized Al₂O₃ nanorods with abundant pentacoordinated Al³⁺ (Al³⁺₅^{penta}) sites. The supported Co on the Al₂O₃ nanorod (Co/Al₂O₃-NR) exhibited higher selectivity (>96% propylene selectivity) and stability (deactivation rate 0.15 h⁻¹), compared to Co supported on an Al₂O₃ nanosheet with fewer pentacoordinated Al³⁺ sites. Various characterizations confirmed that Co(II) mainly exists as CoAl₂O₄ rather than Co₃O₄ in the form of Co/Al₂O₃-NR, which inhibits the reduction of Co(II) to Co0 and improves catalyst stability accordingly.

Keywords: Propane dehydrogenation, metal oxide, alumina, spinel.

1. Introduction

Propane dehydrogenation (PDH) reaction is a production process used in industry to produce propylene. This process has several advantages over the traditional steam cracking/catalytic cracking process, including high propylene selectivity, simple raw material and product composition, and easy separation[1-3]. The development of this process can help address the issue of increasing demand for propylene while also providing significant economic benefits.

Currently, the industry primarily utilizes Pt-Sn catalysts and Cr-based catalysts for propane dehydrogenation. The former is used in the Oleflex process while the latter is utilized in the Catofin process [1,4]. However, due to their high cost and toxicity (in the case of CrO_x), there is ongoing research focused on developing low-cost and environmentally friendly alternatives [5,6].

Co-based catalysts are a promising candidate due to their ability to activate C-H bonds and high selectivity towards olefins [7]. It is believed that the active site of the reaction is Co(II) on the carrier, which promotes propylene desorption. Under high loading conditions, Co₃O₄ can be easily reduced to metallic Co, leading to propylene cracking [8-10]. Stabilizing Co(II) has received significant attention. Yihu Dai et al. [11] synthesized Co/Al₂O₃ using a one-step hydrothermal method. The separated Co²⁺ sites in the resulting catalyst showed high intrinsic activity (specific reaction rate >16 mmol g⁻¹ h⁻¹). The tetrahedral Co²⁺ isolation site was stabilized by γ -Al₂O₃ carrier, promoting propylene desorption and inhibiting coke formation and reduction of active Co sites. Sun et al.[12] found

that at low loadings, "surface spinel" produced by tetrahedral Co^{2+} during the reaction was the active site; large particles of crystalline- Co_3O_4 were formed when loading was high, leading to increased cracking reactions and methane formation. Designing a more suitable carrier for stable $\text{Co}(\text{II})$ species and reducing carbon deposition is necessary.

γ -alumina ($\gamma\text{-Al}_2\text{O}_3$) is commonly used as a catalyst carrier in thermal catalysis due to its large specific surface area, good thermodynamic and chemical stability, among other properties [13,14]. Al_2O_3 contains three different states of Al^{3+} : tetrahedral Al^{3+} ($\text{Al}^{3+}_{\text{tetra}}$), octahedral Al^{3+} ($\text{Al}^{3+}_{\text{oct}}$), and pentacoordinate Al^{3+} ($\text{Al}^{3+}_{\text{penta}}$). The unsaturated pentacoordinate Al^{3+} is located on the surface of Al_2O_3 and can effectively anchor the active phase of the catalyst [15-18]. Liu et al. [19] synthesized stable Ru-CeO_x supported on nano-flower flake Al_2O_3 spheres rich in unsaturated pentacoordinate Al^{3+} which were then used to catalyze the oxidation of propane. Therefore, this paper aims to stabilize $\text{Co}(\text{II})$ through the anchoring effect of pentacoordinate Al^{3+} with the goal of improving stability.

Here, a successful synthesis of Al_2O_3 nanorods ($\text{Al}_2\text{O}_3\text{-NR}$) rich in pentacoordinate Al^{3+} ions was achieved to serve as a support for Co in the PDH reaction. The pentacoordinate Al^{3+} present in the $\text{Al}_2\text{O}_3\text{-NR}$ effectively anchors $\text{Co}(\text{II})$, resulting in the formation of the CoAl_2O_4 spinel phase that exhibits high intrinsic activity and stability. In comparison, samples without pentacoordinate Al^{3+} , such as $\text{Co}(\text{II})$ in $\text{Al}_2\text{O}_3\text{-NS}$, tend to form the Co_3O_4 phase which can be easily reduced to $\text{Co}0$, leading to rapid deactivation of the PDH reaction.

2. Methods and materials

2.1. Catalyst preparation

Al_2O_3 nanosheet was created using a hydrothermal method that had been previously reported. Aluminum nitrate ($\text{Al}(\text{NO}_3)_3\cdot 9\text{H}_2\text{O}$) and urea ($\text{CO}(\text{NH}_2)_2$) were dissolved in deionized water and stirred for 15 minutes until a uniform solution was formed. The concentration of $\text{Al}(\text{NO}_3)_3$ was 0.09 mol/L, with the ratio of $\text{Al}(\text{NO}_3)_3$ to $\text{CO}(\text{NH}_2)_2$ being 1:9. The solution, which had a pH of approximately 4, was then transferred to a PTFE lined stainless steel autoclave and kept at 100°C for 48 hours. After natural cooling, the white precipitate was filtered and washed several times with deionized water and anhydrous ethanol. The powder was dried overnight at 100°C before being calcined in air at a heating rate of 1°C/min for two hours at a temperature of 600°C. This resulted in the creation of Al_2O_3 nanosheet which is referred to as $\text{Al}_2\text{O}_3\text{-NS}$.

The process for creating Al_2O_3 nanorods is similar to that of $\text{Al}_2\text{O}_3\text{-NS}$. The ratio of $\text{Al}(\text{NO}_3)_3$ to $\text{CO}(\text{NH}_2)_2$ remains at 1:9, but the concentration of $\text{Al}(\text{NO}_3)_3$ has been adjusted to 0.2 mol/L. The resulting product is referred to as $\text{Al}_2\text{O}_3\text{-NR}$.

The method used to load Co is the impregnation method. To do this, a specific amount of cobalt nitrate ($\text{Co}(\text{NO}_3)_2\cdot 6\text{H}_2\text{O}$) was dissolved in a small quantity of deionized water and loaded onto two different Al_2O_3 carriers using the constant volume impregnation method. The sample was then left at room temperature for 2 hours, dried overnight at 70°C, and roasted in air at 600°C for 2 hours with a heating rate of 1°C/min. The amount of Co that was impregnated was 5 wt%. The resulting materials were named $\text{Co/Al}_2\text{O}_3\text{-NS}$ and $\text{Co/Al}_2\text{O}_3\text{-NR}$ respectively.

2.2. Catalyst preparation

The X-ray diffraction (XRD) measurement was conducted on a Rigaku C/max-2500 diffractometer using $\text{CuK}\alpha$ radiation filtered through graphite ($\lambda=1.5406\text{ \AA}$), with a 2θ range of 5 to 90°.

The Raman spectrum was acquired using a RenishawinViaReex Raman spectrometer with an Ar ion laser beam of 532 nm at room temperature. The data collection process involved an exposure time of 10 s and 1 accumulation. In the in-situ reaction tank, the inner reaction tank is heated while the outer shell is cooled by cooling water. The gas enters into the void inside the sample tank, flows over the surface of the catalyst in a flooding manner, and then exits. Spectra are collected through the quartz glass window located on top of the sample.

Thermogravimetric analysis (TGA) is conducted using STA449F3 NETZSCH Corp. to examine the carbon deposition of used catalysts. The sample is first preheated in N2 (50 mL/min) at 80°C for half an hour, and then heated in air (100 mL/min) at a speed of 10°C /min until it reaches 800°C.

The laboratory uses self-made equipment to test H₂-TPR and NH₃-TPD. A desiccant is added before the reaction tail gas enters the TCD detector to absorb water produced by the reaction. For H₂-TPR, an appropriate amount of catalyst is treated at 350°C under 30 ml/min N₂ for 20 minutes during the pretreatment stage. Then, high-purity helium is used and the sample is lowered to 50°C. During program temperature reduction stage, a helium switch with a 10% H₂/N₂ mixture maintains a flow rate of 30 ml/min and cuts into the inlet channel of the TCD detector after stabilization of its baseline signal. The heating furnace heats up at a rate of 10°C/min until it reaches 900°C while detecting changes in H₂ signals online using TCD. For NH₃-TPD, dry pretreatment involves placing the sample in a reaction tube and programming temperature from room temperature to reach up to 300°C at a rate of 10°C/min. He gas flow (30 mL/min) purges for about twenty minutes then cools down to around fifty degrees Celsius before introducing mixed gas consisting of ten percent NH₃/He (30 mL/min) for thirty minutes until saturation occurs; finally, desorption attached takes place in He atmosphere heated at ten degrees Celsius per minute until reaching seven hundred degrees Celsius while detecting outgassing through TCD detection method.

A ThermoFisherK-Alpha X-ray photoelectron spectrometer (XPS) from the United States was utilized to examine the valence state and relative content of elements in the catalyst.

The ²⁷Al MAS NMR was measured using a Bruker 400M high-resolution solid-state nuclear magnetic resonance (NMR) spectroscopy with a MAS spin rate of 10 Khz, recovery time of 4 seconds, and pre-scan delay of 6.5 μs.

2.3. Catalyst tests

The PDH catalytic reaction was conducted in a fixed bed reactor under atmospheric pressure. The quartz tubular reactor had an inner diameter of 6 mm and a wall thickness of 1 mm. A catalyst loading mass of 0.2 g was used, with the catalyst being loaded in the middle of the quartz tube. Quartz cotton was filled at both ends of the catalyst, and 0.5 g of quartz sand was added to the front end. The catalyst underwent heating in nitrogen at a rate of 15°C/min until it reached 580°C, followed by pretreatment in H₂ atmosphere for one hour at 580°C before conducting the PDH reaction. During this reaction, C₃H₈:N₂=1:19 and total gas flow rate were maintained at 20 mL/min respectively. An on-line gas chromatograph equipped with TCD detector and flame ionization detector (FID) analyzed C₃H₈, C₃H₆, C₂H₄, C₂H₆ and CH₄ gases; propane conversion rates as well as propylene selectivity were calculated accordingly.

Chromatographic data were analyzed using the FID area normalization method. The propane conversion rate X(C₃H₈), propylene selectivity S(C₃H₆), propylene yield Y(C₃H₆) and propylene space-time yield STY(C₃H₆) were determined using the following formula.

$$X(C_3H_8) = \frac{n(C_3H_8)_{in} - n(C_3H_8)_{out}}{n(C_3H_8)_{in}} \times 100\%$$

$$S(C_3H_6) = \frac{n(C_3H_6)_{out}}{n(C_3H_8)_{in} - n(C_3H_8)_{out}} \times 100\%$$

$$Y(C_3H_6) = S(C_3H_6) \times X(C_3H_8)$$

$$STY(C_3H_6) = \frac{n(C_3H_8)_{in} \times Y(C_3H_6) \times M(C_3H_6)}{V_m \times m_{cat}}$$

Where $n(C_3H_8)_{in}$ represents the molar concentration of propane in the reactants, $n(C_3H_8)_{out}$ represents the molar concentration of propane in the product, $n(C_3H_6)_{out}$ represents the molar concentration of propylene in the product, $M(C_3H_6)$ represents the relative molecular weight of propylene and V_m represents the molar volume of gas (22400 mL/mol). M_{cat} represents the mass of catalyst used in reaction and STY is measured in $kg(C_3H_6) \cdot h^{-1} \cdot kg^{-1}$.

3. Results and Discussion

3.1. Catalytic performances of Co/Al_2O_3 catalysts

Figure 1 displays the catalytic efficiency of Co/Al_2O_3 -NS and Co/Al_2O_3 -NR in PDH reaction. During the initial 4 hours of the reaction, propylene selectivity for both catalysts was between 90.5% to 93.5% and 96% to 97.5%, respectively. Methane, ethane, and ethylene were identified as primary by-products with methane content being relatively high. The Co/Al_2O_3 -NR catalyst exhibited an induction period of approximately one hour where conversion increased from 11% to 40.2%, followed by a slight decrease from 40.2% to 29.8%. (the deactivation constant k_d was found to be at a rate of 0.15 h^{-1}). In comparison with Co/Al_2O_3 -NR, the conversion rate peaked at around 35% for Co/Al_2O_3 -NS catalyst before rapidly decreasing down to 17.3% (the deactivation constant k_d is measured at 0.34 h^{-1}). Conversion rates for Al_2O_3 -NR were slightly higher than those observed in Al_2O_3 -NS while also exhibiting better stability characteristics; indicating that carbon deposits on Al_2O_3 -NR surfaces are less or have better carbon storage capacity when compared with their NS counterparts.

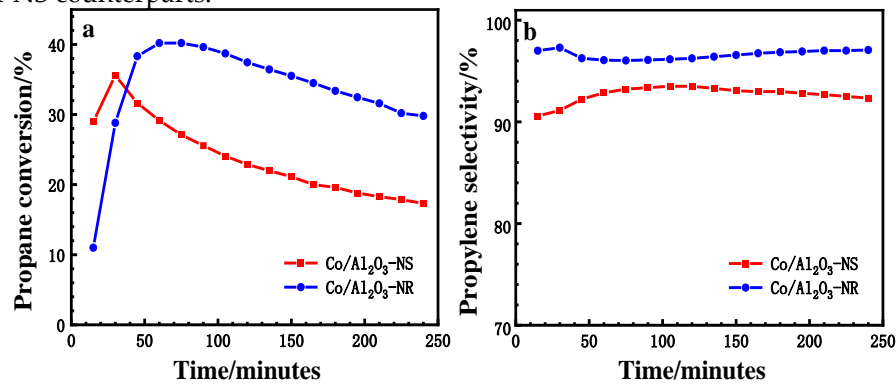


Figure 1. Propane dehydrogenation performance of Co/Al_2O_3 -NS and Co/Al_2O_3 -NR catalysts: (a) conversion; (b) selectivity.^[a]

[a]: Reaction conditions: 0.2 g of catalyst, $C_3H_8 : N_2 = 1:19$, 20 mL/min, $580^\circ C$; pre-treated in H_2 atmosphere for 1 h at $580^\circ C$.

Table 1. Physico-chemical and catalytic properties of Co/Al₂O₃ catalysts.

Catalyst	Y _{propene} , % ^[a]	k _d , h ⁻¹ ^[b]	Carbon deposition, wt% ^[c]
Co/Al ₂ O ₃ -NS	32.4	0.34	9.16
Co/Al ₂ O ₃ -NR	38.6	0.15	7.54

[a] Ypropene represents the yield of propylene, and the maximum yield is listed in the table.

[b] The deactivation rate constant, k_d, was calculated based on the equation, $\ln [(1 - X_{\text{final}}) / X_{\text{final}}] = k_d * t + \ln [(1 - X_{\text{initial}}) / X_{\text{initial}}]$ [20].

[c] Carbon deposition was calculated based on the TGA profile.

Figure 2 displays the activation energies of Co/Al₂O₃-NS and Co/Al₂O₃-NR during the PDH reaction. The apparent activation energy for each was measured at different reaction temperatures: 520°C, 550°C, 580°C, 600°C and 610°C. The results indicate that the apparent activation energy for Co/Al₂O₃-NS was found to be 147.2 kJ/mol while that of Co/Al₂O₃-NR was found to be 202.9 kJ/mol. It is evident from these values that the dehydrogenation energy barrier for Co/Al₂O₃-NR was lower than that of Co/Al₂O₃-NS, making it more favourable towards propane dehydrogenation.

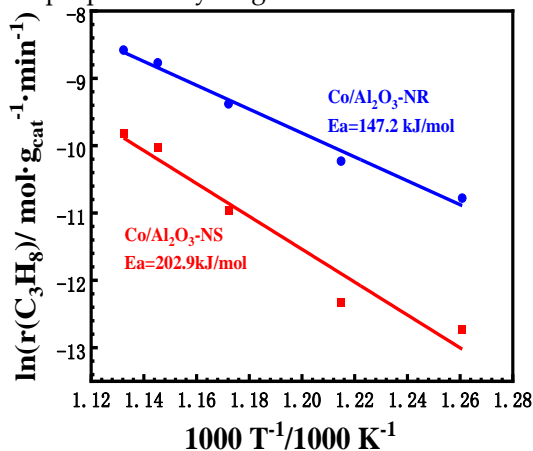


Figure 2. Arrhenius curves and apparent activation energy of Co/Al₂O₃-NS and Co/Al₂O₃-NR catalysts

A Thermogravimetric TGA analysis was conducted on the used catalyst to determine its coke content. The findings are presented in Figure 3. The temperature range of 100°C to 300°C is attributed to the desorption of water molecules from the surface of the catalyst, while 300°C to 600°C corresponds to carbon removal from the catalyst surface [21]. After reaching a temperature above 600°C, the curve remains relatively stable. As shown in Figure 3, Co/Al₂O₃-NS has a higher carbon deposition rate at 9.16% compared with Co/Al₂O₃-NR's rate of only 7.54%. This suggests that high levels of Co₃O₄ on Co/Al₂O₃-NS's surface lead to severe carbon accumulation and rapid deactivation of the catalyst.

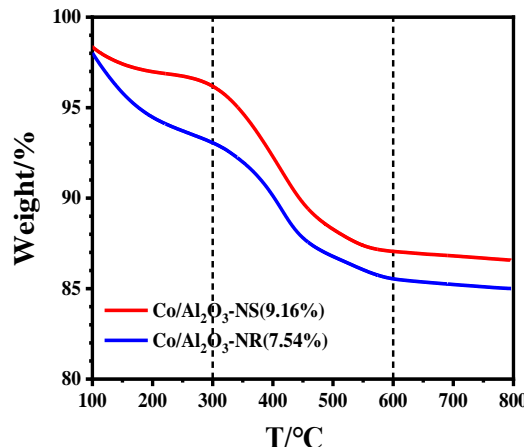


Figure 3. TGA profile of spent Co/Al₂O₃-NS and Co/Al₂O₃-NR catalysts.

3.2. Bulk and surface characterization

To determine the crystal structure and composition information of the material, XRD spectra was used to analyze the catalyst. Figure 4 shows that both Al₂O₃-NS and Al₂O₃-NR detected a peak associated with γ -Al₂O₃ (PDF#29-0063), indicating that the synthesized nanorod Al₂O₃ and nanosheet Al₂O₃ are in γ -Al₂O₃ phase. Additionally, it was observed that the peak height of Al₂O₃-NS is higher than that of Al₂O₃-NR, suggesting that the crystallinity of Al₂O₃-NS is higher. After loading Co, only a peak associated with γ -Al₂O₃ can be detected which indicates that either introduced Co species are uniformly dispersed on the surface of carrier or beyond detection range due to small amount loaded by X-ray diffraction.

The UV-Vis spectra (refer to Figure 4) provides details about the oxidation states and coordination geometry of cobalt species on different morphologies. In the case of Co/Al₂O₃-NR catalysts, two distinct peaks are observed at around 587 nm and 631 nm, which are attributed to the ${}^4A_2 \rightarrow {}^4T_1(P)d-d$ transition of tetrahedral (Td) Co²⁺ (the actual number of characteristic peaks is 3, which may be caused by the insufficient resolution of UV-Vis spectrometers)[8,22]. No other peaks associated with other forms of Co were detected in the spectrum, indicating a normal CoAl₂O₄ spinel structure for the sample. Apart from these two peaks mentioned earlier, the Co/Al₂O₃-NS sample also exhibits two broad absorption bands at around 409 nm and 703 nm respectively. These bands are related to coordination-metal charge transfer between O²⁻ \rightarrow Co²⁺ and O²⁻ \rightarrow Co³⁺ in Co₃O₄. Therefore, it can be concluded that while Co(II) exists mainly as CoAl₂O₄ in Co/Al₂O₃-NR samples; in addition to a small amount of CoAl₂O₄ present in them; large amounts of Co₃O₄ species along with some traces of Co(II) exist within the structure of Co/Al₂O₃-NS samples.

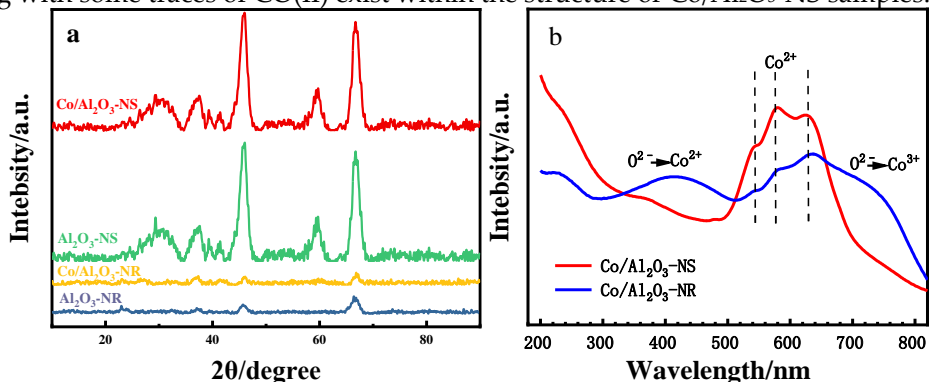


Figure 4. XRD patterns and UV-Vis spectra of Co/Al₂O₃-NS and Co/Al₂O₃-NR catalysts:(a) XRD; (b) UV-Vis.

To analyze the element composition and chemical state of Co/Al₂O₃, X-ray photoelectron spectroscopy (XPS) was used to intercept information related to Co 2p. Figure 5 displays the XPS spectra of the Co 2p electronic energy levels in both catalysts, while Table 2 presents the binding energy and relative surface concentration of Co analyzed by XPS, along with the calculated ratio of Co²⁺/Co³⁺. No peak corresponding to metal Co0 was

observed on either catalyst. The four separate characteristic peaks in all Co 2p nuclear energy level spectra include two spin-orbit double peaks of Co^{2+} and Co^{3+} at positions Co 2p3/2 and 2p1/2, as well as two satellite peaks. The double peaks at position Co 2p3/2 correspond respectively to characteristic peaks of both states [11]. Peak fitting results indicate that surfaces for both types of catalysts are mainly in a state of Co^{2+} ; however, the surface content is higher for $\text{Co}/\text{Al}_2\text{O}_3$ -NR than for $\text{Co}/\text{Al}_2\text{O}_3$ -NS. Additionally, there is a higher ratio between $\text{Co}^{2+}/\text{Co}^{3+}$ on the former's surface compared to that on latter's surface which suggests that it tends more towards forming CoAl_2O_4 .

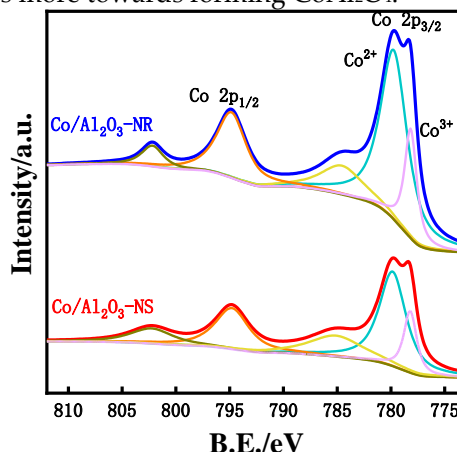


Figure 5. XPS profiles of $\text{Co}/\text{Al}_2\text{O}_3$ -NS and $\text{Co}/\text{Al}_2\text{O}_3$ -NR catalysts

Table 2. XPS results of $\text{Co}/\text{Al}_2\text{O}_3$ -NS and $\text{Co}/\text{Al}_2\text{O}_3$ -NR catalysts.

Catalyst	Surface concentration		$\text{Co}^{2+}/\text{Co}^{3+}$ mol- lar ratio	Binding energy (eV)
	Co, mol %	Co, wt%		
$\text{Co}/\text{Al}_2\text{O}_3$ -NS	1.89	5.90	3.03	779.5
$\text{Co}/\text{Al}_2\text{O}_3$ -NR	3.29	11.31	3.56	779.4

Figure 6 displays the Raman spectrum of each catalyst. $\text{Co}/\text{Al}_2\text{O}_3$ -NS exhibits a clear Co_3O_4 structure and five Raman activity modes: A_{1g} (680 cm^{-1}), F_{2g} (616 cm^{-1} , 523 cm^{-1} , 191 cm^{-1}), E_g (480 cm^{-1}) [23,24]. No peaks related to Al_2O_3 or other Co phases are present. In comparison, $\text{Co}/\text{Al}_2\text{O}_3$ -NR also has peaks corresponding to the Co_3O_4 structure at 680 cm^{-1} and 191 cm^{-1} . Additionally, there are peaks belonging to the CoAl_2O_4 structure that correspond to F_{2g} (607 cm^{-1} , 191 cm^{-1}) and E_g (480 cm^{-1}) [25]. The peak of CoAl_2O_4 is difficult to observe due to its weak intensity and coverage by Co_3O_4 . The A_{1g} peak in the figure shows that the peak value of $\text{Co}/\text{Al}_2\text{O}_3$ -NR is significantly smaller than that of $\text{Co}/\text{Al}_2\text{O}_3$ -NS indicating that less surface area on $\text{Co}/\text{Al}_2\text{O}_3$ -NR contains Co_3O_4 and its main component is CoAl_2O_4 .

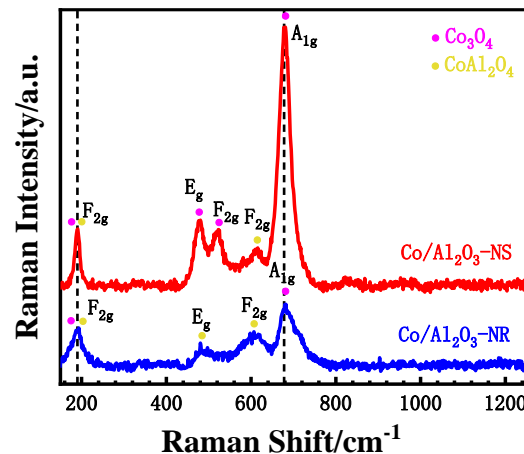


Figure 6. Raman spectra of Co/Al₂O₃-NS and Co/Al₂O₃-NR catalysts.

From the above characterization, it is easy to see that in the Co/Al₂O₃-NS catalyst, Co(II) mainly exists in the form of Co₃O₄, which leads to the rapid deactivation of the catalyst. In contrast, the Co/Al₂O₃-NR catalyst has a small amount of Co₃O₄ and mostly consists of stable spinel structure (CoAl₂O₄), leading to improved stability. To understand the difference between these two catalysts, ²⁷Al MAS NMR spectra were analyzed. Pure Al₂O₃ without Co showed only two different Al species in Al₂O₃-NS: octahedral Al³⁺ at about 4.13 ppm and tetrahedral Al³⁺ at about 61.8 ppm. However, in addition to these peaks, there was also a characteristic peak at about 30.7 ppm in Al₂O₃-NR attributed to pentacoordinate Al³⁺ ions (~18.5%)[26,27]. With the addition of Co, the peak corresponding to the pentacoordinate Al³⁺ ion disappeared and most of the peaks were converted into tetrahedral Al³⁺ ions. This indicates that after being impregnated, the Co particles first occupied the pentacoordinate Al³⁺ position on the surface of Al₂O₃. The disappearance of the Co-loaded NMR peak confirms that this peak is designated as Al³⁺ ions located on the surface of the Al₂O₃ support rather than lattice defect sites uniformly distributed in bulk phase[28]. The pentacoordinate Al³⁺ can anchor active centers, maintain high dispersion and thermal stability. Co(II) loaded onto a pentacoordinate Al³⁺ site on an Al₂O₃ surface is well anchored to prevent formation of a Co₃O₄ phase, which is consistent with Raman spectrum results.

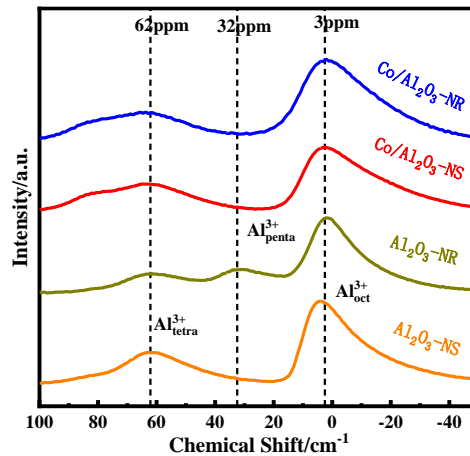


Figure 7. ²⁷Al MAS NMR spectra of Al₂O₃ and Co/Al₂O₃ catalysts.

Table 3. The proportion of different coordination Al^{3+} calculated from the peak area of ^{27}Al MAS NMR spectra.

Catalysts	Al ³⁺ coordination/%		
	Tetrahedral Al	Pentacoordinate Al	Octahedral Al
Al ₂ O ₃ -NS	31.5	—	68.4
Al ₂ O ₃ -NR	17.2	18.5	64.3
Co/Al ₂ O ₃ -NS	33.8	—	66.1
Co/Al ₂ O ₃ -NR	29.4	—	70.6

The SEM images of the Al₂O₃ support and Co-based catalyst after loading are presented in Figure 8. The Al₂O₃-NR support used in this study has a regular long rod-shaped structure, while the Al₂O₃-NS exhibits a regular sheet-like structure. Upon impregnation with 5%wt Co, there was no significant change observed on the surface of the Co/Al₂O₃-NS catalyst, and its main layered structure remained intact. On the other hand, for Co/Al₂O₃-NR, the main structure still consisted of nanorods with aggregated Co oxide particles appearing at both ends of these nanorods.

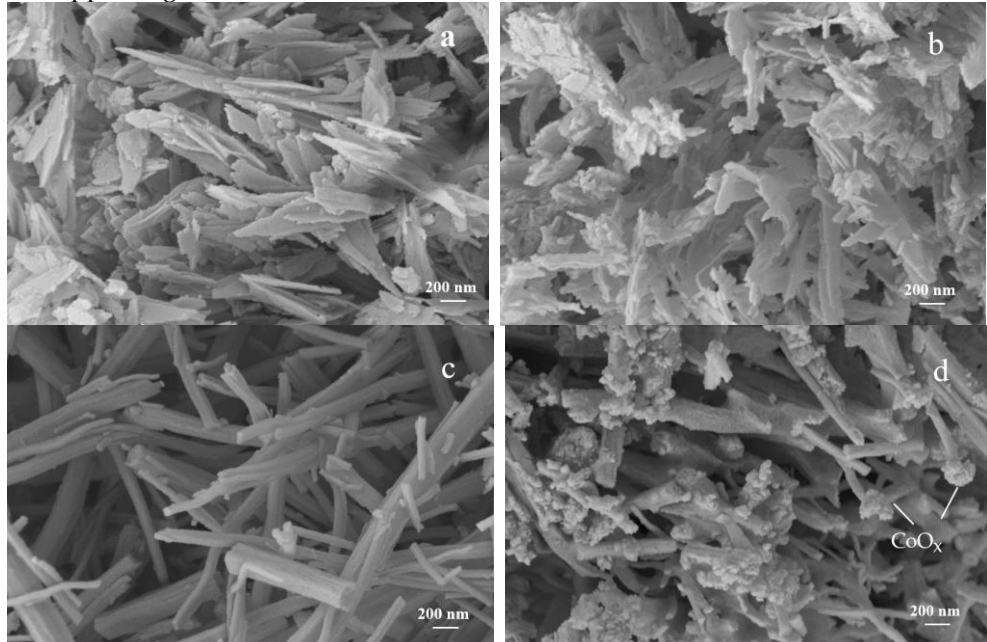


Figure 8. SEM images of catalysts: (a) Al₂O₃-NS; (b) Co/Al₂O₃-NS; (c) Al₂O₃-NR; (d) Co/Al₂O₃-NR.

3.3. Reducing ability and acidity of the catalysts

H_2 -TPR was used to examine how oxidized Co species in two $\text{Co}/\text{Al}_2\text{O}_3$ catalysts (Figure 9) behave during reduction. The $\text{Co}/\text{Al}_2\text{O}_3$ -NS catalyst has two reduction peaks at 450 $^{\circ}\text{C}$ and 640 $^{\circ}\text{C}$, which correspond to the reduction of Co_3O_4 to CoO and the reduction of CoO to Co^{0} , respectively. On the other hand, the peaks of $\text{Co}/\text{Al}_2\text{O}_3$ -NR that correspond to the reduction of Co_3O_4 are located at lower temperatures 420 $^{\circ}\text{C}$ and 598 $^{\circ}\text{C}$. A comparison between these two catalysts shows that there is a stronger interaction between Co and Al_2O_3 -NR under pentacoordinate Al^{3+} ions' influence as evidenced by the shift in position for peak temperature towards higher values for $\text{Co}/\text{Al}_2\text{O}_3$ -NS. Additionally, it is evident that there is less content of Co_3O_4 on the surface of $\text{Co}/\text{Al}_2\text{O}_3$ -NR compared with that on $\text{Co}/\text{Al}_2\text{O}_3$ -NS since its peak temperature for reducing this compound is much lower; thus indicating a tendency for formation into a spinel structure consisting mainly of $\text{Co}^{(II)}$ and CoAl_2O_4 .

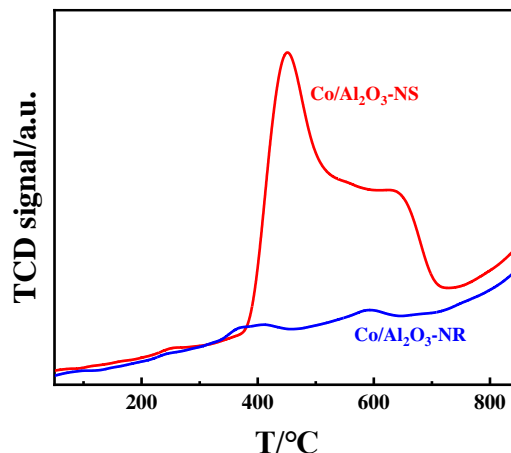


Figure 9. H_2 -TPR profiles of $\text{Co}/\text{Al}_2\text{O}_3$ -NS and $\text{Co}/\text{Al}_2\text{O}_3$ -NR catalysts.

Figure 10 displays the results obtained from NH_3 -TPD, while Table 4 presents the ratios of various acid strengths. The Al_2O_3 support exhibits weak and strong acids at approximately 160 $^{\circ}\text{C}$ and 450 $^{\circ}\text{C}$, respectively. Upon Co loading, a medium-strength acid emerges on the surface of $\text{Co}/\text{Al}_2\text{O}_3$ -NR and $\text{Co}/\text{Al}_2\text{O}_3$ -NS around 215 $^{\circ}\text{C}$. Furthermore, the strong acid present on $\text{Co}/\text{Al}_2\text{O}_3$ -NS's surface is significantly stronger than that found on $\text{Co}/\text{Al}_2\text{O}_3$ -NR's surface, which could be another explanation for their varying carbon deposition rates.

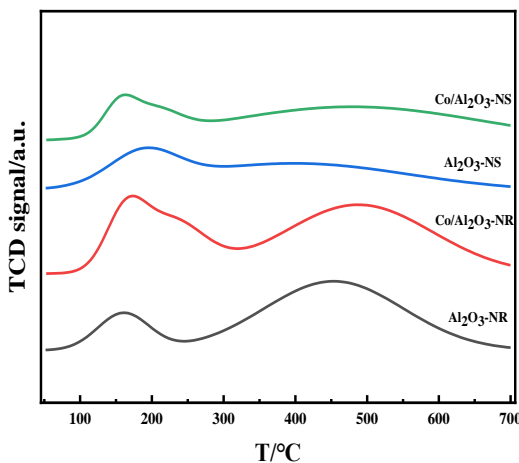


Figure 10. NH_3 -TPD profiles of $\text{Co}/\text{Al}_2\text{O}_3$ -NS and $\text{Co}/\text{Al}_2\text{O}_3$ -NR catalysts.

Table 4. The proportion of different acid sites calculated from the peak area of NH₃-TPD.

Catalysts	Acid sites/%		
	Strong acid sites	Medium strong acid sites	Weak acid sites
Al ₂ O ₃ -NS	74.8	—	25.2
Al ₂ O ₃ -NR	83.4	—	16.6
Co/Al ₂ O ₃ -NS	79.2	12.4	8.4
Co/Al ₂ O ₃ -NR	64.5	22.4	13.1

3.4. Discussion

The Co/Al₂O₃-NR catalyst exhibits superior selectivity and stability in the propane dehydrogenation reaction compared to Co/Al₂O₃-NS. During a 4-hour activity test, the inactivation rate of Co/Al₂O₃-NR was only 0.15 h⁻¹, significantly lower than that of Co/Al₂O₃-NS, indicating higher stability. To investigate this difference in stability between the two catalysts, we analyzed carbon deposition on spent catalyst using thermogravimetry (TGA). The results showed that carbon deposition was 7.54% for Co/Al₂O₃-NR and 9.16% for Co/Al₂O₃-NS. Additionally, NH₃-TPD characterization revealed that Co/Al₂O₃-NS had a higher proportion of strong acid sites which led to greater carbon deposition and faster deactivation compared to Co/Al₂O₃-NR. These characterizations demonstrate that surface carbon deposition is the primary cause of catalyst deactivation.

The UV-Vis and Raman spectra indicate that Co(II) in Co/Al₂O₃ undergoes partial oxidation to form Co₃O₄. This is subsequently reduced to CoO, then to metallic Co0 (as evidenced by H₂-TPR data). The presence of metallic Co0 leads to propylene cracking and carbon deposition on the catalyst surface. In contrast, when interacting with Al₂O₃, Co(II) in Co/Al₂O₃-NR forms a stable spinel phase called CoAl₂O₄. Compared to Co₃O₄, this spinel phase is less easily reduced (the reduction peak for the spinel in H₂-TPR occurs above 700°C). The UV-Vis spectrum shows that while there is some amount of the spinel phase present on the surface of the catalyst in both types (NS and NR), it mainly exists as Co₃O₄. This conclusion is supported by an A_{1g} peak at 680 cm⁻¹ observed in the Raman spectrum. Based on H₂ consumption during H₂-TPR analysis, only a small amount of Co₃O₄ exists in the NR catalyst; most of it exists as stable structured-CoAl₂O₄. Therefore, two states exist for cobalt: one as unstable metallic-Co0 from easily reducible-Co₃O₄ found mostly in NS catalysts leading to deactivation due to carbon deposition; and another state as stable structured-CoAl₂O₄ from less-reducible-spinels found mostly in NR catalysts which do not cause deactivation.

We have analyzed the reasons behind the formation of different Co(II) species. Our analysis suggests that the variation in surface coordination of Al₂O₃ carriers results in distinct binding energies between Co(II) and Al₂O₃, leading to two different structures: CoAl₂O₄ and Co₃O₄. The ²⁷Al MAS NMR spectrum indicates two states of Al³⁺ on the Al₂O₃-NS carrier - tetrahedral and octahedral - while pentacoordinate Al³⁺ is present as a defect site on the surface of the Al₂O₃-NR carrier. Upon loading, Co(II) preferentially binds to pentacoordinate Al³⁺, resulting in spinel phase formation of CoAl₂O₄. This phase is more

stable than the Co_3O_4 phase as an active catalyst and less susceptible to reduction by H_2 gas.

4. Conclusions

Two different morphologies of Al_2O_3 were synthesized using the hydrothermal method and then loaded with 5 wt% Co for propane dehydrogenation reaction. The results showed that Co/ Al_2O_3 -NR exhibited higher selectivity and stability compared to Al_2O_3 -NS. This is because Al_2O_3 -NR contains a higher amount of pentacoordinate Al^{3+} which can stabilize $\text{Co}(\text{II})$ particles, forming more stable active phase CoAl_2O_4 spinel that is not easily reduced by H_2 . On the other hand, the surface of Al_2O_3 -NS does not contain pentacoordinate Al^{3+} , resulting in mainly Co_3O_4 as an active phase. However, this phase is easily reduced to metallic Co_0 leading to cracking reactions and carbon deposition. In conclusion, modifying the support morphology can further improve the activity and stability of Co-based PDH catalysts.

Author Contributions: Conceptualization, Zhiping Zhao and Weiyu Song; methodology, Zhiping Zhao; validation, Zhiping Zhao, Yanbing Tong and Jinru Sun.; investigation, Zhiping Zhao.; resources, Ming Ke.; writing—original draft preparation, Zhiping Zhao.; writing—review and editing, Ming Ke.; visualization, Zhiping Zhao; supervision, Ming Ke and Weiyu Song.; project administration, Zhiping Zhao and Ming Ke; funding acquisition, Ming Ke. All authors have read and agreed to the published version of the manuscript.

Funding: This research was funded by National Natural Science Foundation of China, grant number 21776303.

Data Availability Statement: The data presented in this study are available on request from the corresponding author.

Acknowledgments: This work acknowledges the financial support from the National Natural Science Foundation of China (21776303). The authors are indebted to the State Key Laboratory of Heavy Oil Processing (China University of Petroleum) for the SEM, Raman, XPS and XRD measurements.

Conflicts of Interest: The authors declare no conflict of interest.

References

1. Jesper J. H. B. Sattler, Javier Ruiz-Martinez, Eduardo Santillan-Jimenez, Bert M. Weckhuysen. Catalytic Dehydrogenation of Light Alkanes on Metals and Metal Oxides. *Chem. Rev.*, 2014, 114, 10613-10653.
2. Eric McFarland. Unconventional Chemistry for Unconventional Natural Gas. *Science*, 2012, 338, 340-342.
3. C. A. Carrero, R. Schloegl, I. E. Wachs, R. Schomaecker. Critical Literature Review of the Kinetics for the Oxidative Dehydrogenation of Propane over Well-Defined Supported Vanadium Oxide Catalysts. *ACS Catal.*, 2014, 4, 3357-3380.
4. Bipin V. Vora. Development of Dehydrogenation Catalysts and Processes. *Top Catal.*, 2012, 55, 1297-1308.
5. Odd A. Barrias, Anders Holmen, Edd A. Blekkan. Propane Dehydrogenation over Supported Pt and Pt-Sn Catalysts: Catalyst Preparation, Characterization, and Activity Measurements. *J. Catal.*, 1996, 158, 1-12.
6. Derossi S., Ferraris G., Fremiotti S., Garrone E., Ghiotti G., Campa M. C., Indovina V. Propane Dehydrogenation on Chromia/Silica and Chromia/Alumina Catalysts. *J. Catal.*, 1993, 148, 36-46.
7. Marc Moselage, Jie Li, Lutz Ackermann. Cobalt-Catalyzed C-H Activation. *ACS Catal.*, 2016, 6, 498-525.
8. Bo Hu, Wun-Gwi Kim, Taylor P. Sulmonetti, Michele L. Sarazen, Shuai Tan, Jungseob So, Yujun Liu, Ravindra S. Dixit, Sankar Nair, Christopher W. Jones. Mesoporous CoAl_2O_4 Spinel Catalyst for Non-Oxidative Propane Dehydrogenation. *ChemCatChem*, 2017, 9(17), 3330-3337.
9. Xiuyi Li, Pengzhao Wang, Haoren Wang, Chunyi Li. Effects of the state of Co species in Co/ Al_2O_3 catalysts on the catalytic performance of propane dehydrogenation. *Appl. Surf. Sci.*, 2018, 441, 688-693.
10. N. Dewangan, J. Ashok, M. Sethia, S. Das, S. Pati, K. Hidajat, S. Kawi. Cobalt-based catalyst supported on different morphologies of alumina for non-oxidative propane dehydrogenation: Effect of metal support interaction and Lewis acidic sites. *ChemCatChem*, 2019, 11(19), 4923-4934.
11. Yihu Dai, Jingjing Gu, Suyang Tian, Yue Wu, Junchao Chen, Fanxing Li, Yonghua Du, Luming Peng, Weiping Ding, Yanhui Yang. γ - Al_2O_3 sheet-stabilized isolate Co^{2+} for catalytic propane dehydrogenation. *Journal of Catalysis*, 2020, 381, 482-492.
12. Yanan Sun, Yimin Wu, Honghong Shan, Chunyi Li. Studies on the Nature of Active Cobalt Species for the Production of Methane and Propylene in Catalytic Dehydrogenation of Propane. *Catal. Lett.*, 2019, 145, 1413-1419.
13. Pengzhao Wang, Zhikang Xu, Tinghai Wang, Yuanyuan Yue, Xiaojun Bao, Haibo Zhu. Unmodified bulk alumina as an efficient catalyst for propane dehydrogenation. *Catal. Sci. Technol.*, 2020, 10, 3537-3541.

14. Zean Xie, Zhi Li, Peng Tang, Yangyang Song, Zhen Zhao, Lian Kong, Xiaoqiang Fan, Xia Xiao. The effect of oxygen vacancies on the coordinatively unsaturated Al-O acid-base pairs for propane dehydrogenation. *J. Catal.*, 2021, 397, 172-182.
15. Xinwei Yang, Qing Li, Erjun Lu, Zhiqiang Wang, Xueqing Gong, Zhiyang Yu, Yun Guo, Li Wang, Yanglong Guo, Wangcheng Zhan, Jinshui Zhang, Sheng Da. Taming the stability of Pd active phases through a compartmentalizing strategy toward nanostructured catalyst supports. *Nat. Commun.*, 2019, 10, 1611.
16. Huimei Duan, Rui You, Shutao Xu, Zhaorui Li, Kun Qian, Tian Cao, Weixin Huang, Xinhe Bao. Pentacoordinated Al³⁺-Stabilized Active Pd Structures on Al₂O₃-Coated Palladium Catalysts for Methane Combustion. *Angew. Chem. Int. Ed.*, 2019, 58, 12043-12048.
17. Ja Hun Kwak, Jianzhi Hu, Donghai Mei, Cheol-Woo Yi, Do Heui Kim, Charles H. F. Peden, Lawrence F. Allard, Janos Szanyi. Coordinatively Unsaturated Al³⁺ Centers as Binding Sites for Active Catalyst Phases of Platinum on γ -Al₂O₃. *Science*, 2009, 325, 1670-1673.
18. Lei Shi, Gaoming Deng, Wencui Li, Shumiao, Qingnan Wang, Weiping Zhang, Anhui Lu. Al₂O₃ Nanosheets Rich in Pentacoordinate Al³⁺ Ions Stabilize Pt-Sn Clusters for Propane Dehydrogenation. *Angew. Chem. Int. Ed.*, 2015, 54, 13994-13998.
19. Wenming Liu, Shenyu Yang, Qiuli Zhang, Tianyao He, Yimei Luo, Jinxiong Tao, Daishe Wu, Honggen Peng. Insights into flower-like Al₂O₃ spheres with rich unsaturated pentacoordinate Al³⁺ sites stabilizing Ru-CeO_x for propane total oxidation. *Appl. Catal. B*, 2021, 292, 120171.
20. Namgi Jeon, Okkyun Seo, Jungmok Oh, Jisu Park, Iljun Chung, Jaemyung Kim, Osami Sakata, Akhil Tayal, Yongju Yun. Non-oxidative propane dehydrogenation over alumina-supported Co-V oxide catalysts. *Appl. Catal. A*, 2021, 614, 118036.
21. Yihu Dai, Yue Wu, Hua Dai, Xing Gao, Suyang Tian, Jingjing Gu, Xianfeng Yi, Anmin Zheng, Yanhui Yang. Effect of coking and propylene adsorption on enhanced stability for Co²⁺-catalyzed propane dehydrogenation. *J. Catal.*, 2021, 395, 105-116.
22. Marcos Zayat, David Levy. Blue CoAl₂O₄ Particles Prepared by the Sol-Gel and Citrate-Gel Methods. *Chem. Mater.*, 2000, 12, 2763-2769.
23. V. G. Hadjiev, M. N. Iliev, I. V. Vergilov. The Raman spectra of Co₃O₄. *J. Phys. C*, 1988, 21, L199-L201.
24. Beatriz Rivas-Murias, Verónica Salgueiriño. Thermodynamic CoO-Co₃O₄ crossover using Raman spectroscopy in magnetic octahedron-shaped nanocrystals. *J. Raman Spectrosc.*, 2017, 48, 837-841.
25. C. M. Alvarez-Docio, J. J. Reinosa, A. Del Campo, J. F. Fernandez. Investigation of thermal stability of 2D and 3D CoAl₂O₄ particles in core-shell nanostructures by Raman spectroscopy. *J. Alloys Compd.*, 2019, 779, 244-254.
26. F. R. Chen, J. G. Davis, J. J. Fripiat. Aluminum Coordination and Lewis Acidity in Transition Aluminas. *J. Catal.*, 1992, 133, 263-278.
27. John J. Fitzgerald, Gilberto Piedra, Steven F. Dec, Mark Seger, Gary E. Maciel. Dehydration Studies of a High-Surface-Area Alumina (Pseudo-boehmite) Using Solid-State ¹H and ²⁷Al NMR. *J. Am. Chem. Soc.*, 1997, 119, 7832-7842.
28. Ja Hun Kwak, Jian Zhi Hu, Do Heui Kim, Janos Szanyi, Charles H.F. Peden. Penta-coordinated Al³⁺ ions as preferential nucleation sites for BaO on γ -Al₂O₃: An ultra-high-magnetic field ²⁷Al MAS NMR study. *J. Catal.*, 2007, 251, 189-194.